Limnol. Oceanogr., 48(3), 2003, 971–982

Horizontal transport and dispersion in the surface layer of a medium-sized lake

Roman Stocker and Jörg Imberger
Centre for Water Research, University of Western Australia, 35 Stirling Highway, 6009 Crawley, Western Australia, Australia

Abstract

Lagrangian GPS drifter experiments, carried out in the surface layer of stratified Lake Kinneret (Israel), are presented. Differential kinematic properties and Lagrangian statistics were calculated and used to estimate the dominant mechanisms for horizontal dispersion. On time scales smaller than a few internal wave periods, internal waves lead to strong divergence and convergence events, causing instantaneous apparent horizontal growth rates that were larger, by up to an order of magnitude, than the actual mean dispersion coefficient. It is shown that the internal wave field modulated the vorticity field so as to satisfy conservation of potential vorticity. On time scales larger than a few internal wave periods, unbounded horizontal shear dispersion was of the same order as the actual mean observed dispersion coefficient ($K_{xy} = 17.1$ m^2 s^{-1}), while vertical shear dispersion was negligible.

In a stratified lake, the surface layer is where most primary production takes place. Knowledge of the processes responsible for horizontal dispersion is therefore of key importance in understanding the biological dynamics of a lake. Small- to medium-sized lakes, in particular, are of ubiquitous nature and importance. Despite this, very few horizontal dispersion studies exist for lakes of these sizes, and those that do exist are often limited to the hypolimnion (Quay et al. 1979; Peeters 1994; Lawrence et al. 1995; Peeters et al. 1996). The size of a lake is interpreted here in terms of the effect of the Earth's rotation on the lake's response to external disturbances, summarized by the Burger number $S = c/Lf$ (Antenucci and Imberger 2001), where c is the nonrotating internal wave phase speed, f the Coriolis frequency, and L the horizontal dimension of the lake. In large lakes and in the ocean, rotation confines the motion to the boundaries ($S \to 0$), in medium lakes it influences the basin-scale response through a balance with stratification (S is $O(1)$), while in small lakes rotational effects are negligible ($S \to \infty$).

While so far no evidence exists that the Burger number directly affects dispersion processes, it will be shown that large-scale divergence and convergence events are associated with the internal wave field, whose shape and amplitude are in turn strongly dependent on the Burger number. For example, Antenucci et al. (2000) presented the seasonal evolution of the internal wave field in terms of the Burger number, finding that resonance conditions can be established as the stratification changes, while Stocker and Imberger (in press) showed that the partitioning of energy between waves and non–wave-like motions is governed by the Burger number.

Field studies commonly lump all mechanisms responsible for horizontal dispersion into a single empirical law relating the rate of growth of a tracer cloud, or dispersion coefficient, to its size (Okubo 1971; Murthy 1976; Lawrence et al. 1995). In this respect, a unifying approach has been introduced by Okubo (1971): by converting measured distributions into equivalent radially symmetric ones, whose variance is σ_r^2, a standard reference scale for dispersion is defined as $d_r = 3\sigma_r$. An apparent dispersion coefficient is computed from the elapsed time t as

$$K_a = \frac{\sigma_r^2}{4t} \tag{1}$$

and usually reported as a function of d_r in the form

$$K_a = \alpha d_r^{\beta} \tag{2}$$

For the surface layer, Lawrence et al. (1995) combined data from several oceanic studies presented in Okubo (1971) with results by Murthy (1976) for Lake Ontario and with their own data from a very small lake, finding $\alpha = 3.20 \times 10^{-4}$ m$^{0.9}$ s^{-1} (the fractional exponent is dimensionally required) and $\beta = 1.10$, for scales d_r ranging from 10 to 10^5 m. While the outcomes of such investigations are of considerable practical usefulness (Lawrence et al. 1995; Sundermeyer and Ledwell 2001), they can lead to misinterpretations of the mechanisms underlying dispersion (Murthy 1975) and ''must remain provisional until the physical processes giving rise to diffusion are well understood,'' as pointed out by Okubo (1971).

The growth of a tracer cloud in the surface layer is governed by several mechanisms. Irreversible spreading, or dispersion, is caused by fluctuations in the velocity field at scales smaller than the cloud that contribute to the cloud's growth in the form of turbulent dispersion (Fischer et al. 1979); by horizontal velocity gradients in the flow field at scales larger than the cloud that together with small-scale horizontal fluctuations cause horizontal shear dispersion (Fischer et al. 1979); and by vertical gradients in the flow field, which associated with small-scale vertical fluctuations yield

Acknowledgments

The field experiments were funded by the Israeli Water Commission, via the Kinneret modeling project, conducted jointly by the Kinneret Limnological Laboratory and the Centre for Water Research. The support of the Kinneret Limnological Laboratory and Centre for Water Research field staff is gratefully acknowledged. The help of Penny Van Reenen, Peter Yeates, and Andres Gomez in conducting the field experiments is gratefully acknowledged. Thanks to Craig Stevens, Bernard Laval, David Johnson, and two anonymous reviewers for comments on the manuscript. R.S. gratefully acknowledges Ing. Guglielmo Marin and Ing. Aldo Gini scholarships. This paper forms Centre for Water Research reference ED 1626-RS.

Table 1. Details of the six drifter experiments carried out in Lake Kinneret in 2001. T_{exp} is the duration of the experiment and T_{tot} the total number of drifter hours available. Drifters 1 to 4 were drogued at 5-m depth, drifter 5 at 2.5 m, and drifter 6 at 8 m (experiment 5) and 8.5 (experiment 6). Deployment and retrieval are given in local time and refer to year 2001.

Experiment	Drifters	Deployment	Retrieval	T_{exp} (h)	T_{tot} (h)
1	1,2,3,4	1855 h, 23 April	0700 h, 25 April	36	81
2	1,2,3,4	1945 h, 29 April	1030 h, 1 May	39	155
3	1,3,4	2135 h, 2 May	0820 h, 6 May	82	248
4	1,2,3,4	2200 h, 8 May	0910 h, 11 May	57	228
5	1,2,3,4,5,6	0920 h, 19 June	0810 h, 22 June	94.5	567
6	1,2,3,4,5,6	1800 h, 24 June	0845 h, 2 July	183	653

vertical shear dispersion (Bowden 1965). A comprehensive understanding of horizontal dispersion requires a separate quantification of each of these mechanisms.

For short times, in the order of a day, it will be shown that the horizontal extent of a cloud is dramatically affected by internal wave-driven divergence and convergence events. As an internal wave propagates, the thermocline rises and falls, causing divergent and convergent flows in the surface layer, respectively. Murthy (1975) found that such convergence events are capable of masking the dispersive action of turbulence when only the horizontal extent of the cloud is measured. Stocker and Imberger (2003) showed that the superposition of internal waves upon a steady geostrophic flow can enhance horizontal dispersion for small values of the Burger number (medium-sized lakes), a mechanism they called *pseudochaotic advection,* that can be dominant over turbulent dispersion for large clouds and large time scales. Despite these considerations, the effects of basin-scale internal waves on the growth of a cloud are still lacking field verification.

In order to quantify the dominant horizontal dispersion mechanisms, with particular focus on the role of internal waves, GPS-tracked drifters were released during stratified conditions in the surface layer of Lake Kinneret (Israel), a lake of medium size ($S \approx 0.65$). Interestingly, no other comprehensive drifter studies have been carried out so far in small- to medium-sized lakes, while other environments have been extensively investigated, from the deep (Freeland et al. 1975; Krauss and Böning 1987; Richez 1998) to the near-surface ocean (Colin de Verdiere 1983; Poulain and Niiler 1989; Paduan and Niiler 1993; Sanderson 1995), coastal regions (List et al. 1990), the coastal transition zone (Haynes and Barton 1991), channels (Dever et al. 1998), and very large lakes (Csanady 1963; Murthy 1975, 1976; Sanderson and Okubo 1986; Palmer et al. 1987; Sanderson 1987; Muzzi and McCormick 1994; Okumura and Endoh 1995; Pal et al. 1998).

Drifters have both advantages and disadvantages when compared to tracers. Drifter studies are characterized by a greater experimental flexibility and the possibility of a much higher sampling frequency, due to improvements in tracking technology over recent years. On the other hand, tracers include spreading due to vertical shear dispersion and therefore represent the total fate of a diffusive substance (Peeters 1994). Thus, since drifters are not subject to vertical shear dispersion, they are representative of the behavior of diffusive substances only when vertical shear dispersion is small compared to horizontal shear dispersion. As will be shown, this was in fact the case in our study. It is worth noting that, while a drifter drogued at a fixed depth in a stratified environment does not in general represent the flow field appropriately because it is unable to follow the vertical excursions of the isopycnals, this limitation does not apply to the surface layer, which is typically well mixed and of approximately uniform velocity.

The development of a substantial body of theory allows the extraction of a wide range of information from single trajectories (Colin de Verdiere 1983; Haynes and Barton 1991) as well as from clusters of drifters (Molinari and Kirwan 1975; Okubo and Ebbesmeyer 1976; Sanderson 1995), even for small numbers of drifters (often 4 to 10). Cluster analysis (Molinari and Kirwan 1975; Okubo and Ebbesmeyer 1976; Sanderson 1987) was applied for the first time to drifter experiments in a lake, allowing the determination of Lagrangian velocity gradients and smaller scale, residual motions. This information, used in conjunction with simple models from the literature, provided insight into the dominant mechanisms governing the growth of a cloud.

The field experiment

The data—Six drifter experiments (Table 1) were carried out in the surface layer of Lake Kinneret between spring and summer of 2001. Lake Kinneret (Israel, 32°50′N, 35°35′E) has a compact, elliptical shape, 20 km in length and 10 km in width (Fig. 1). At the time of these experiments, the water level was 213 m below mean sea level, resulting in a surface area of 161 km^2, a volume of 3.7 km^3, a maximum depth of 39 m, and an average depth of 22.7 m (*see* fig. 2 in Serruya 1975).

The drifters, described by Johnson et al. (pers. comm.), were deployed at different locations in the lake, with a focus on the western shallows. They were drogued at depths between 2.5 and 8.5 m (Table 1). The sampling frequency was 0.1 Hz and the precision was 10-m horizontal root mean square. The error on the relative position of two drifters has been estimated from separate tests to be less than 5 m (95% confidence). Discrepancies between the motion of the drifters and that of water parcels caused by factors such as wind-

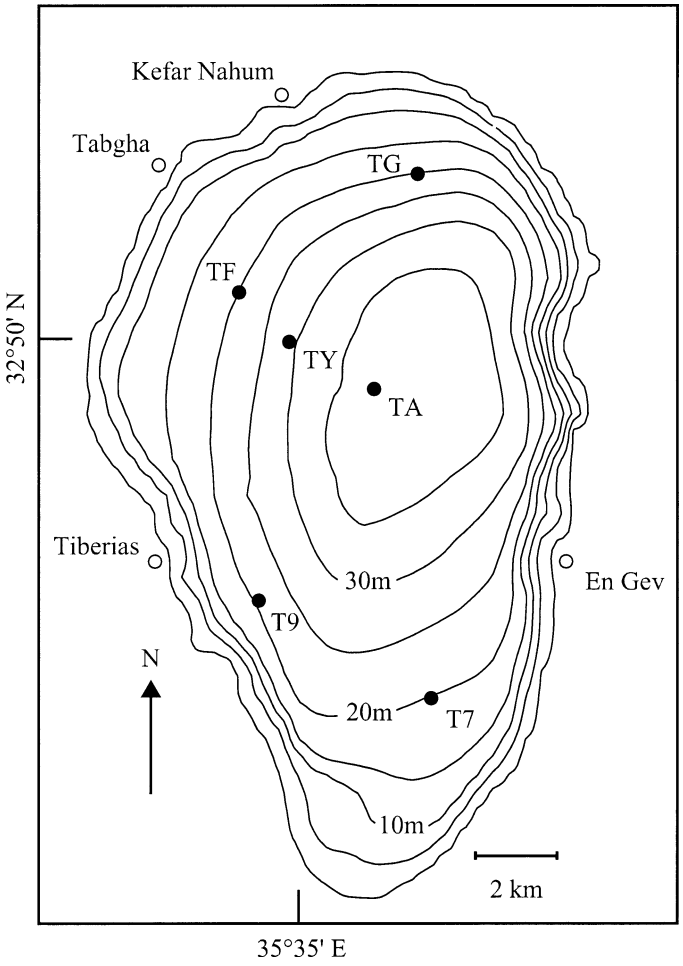

Fig. 1. Map of Lake Kinneret. The six stations in the lake (circles) measured water column temperatures and wind speed and direction. In addition, wind was measured at Tabgha and En Gev.

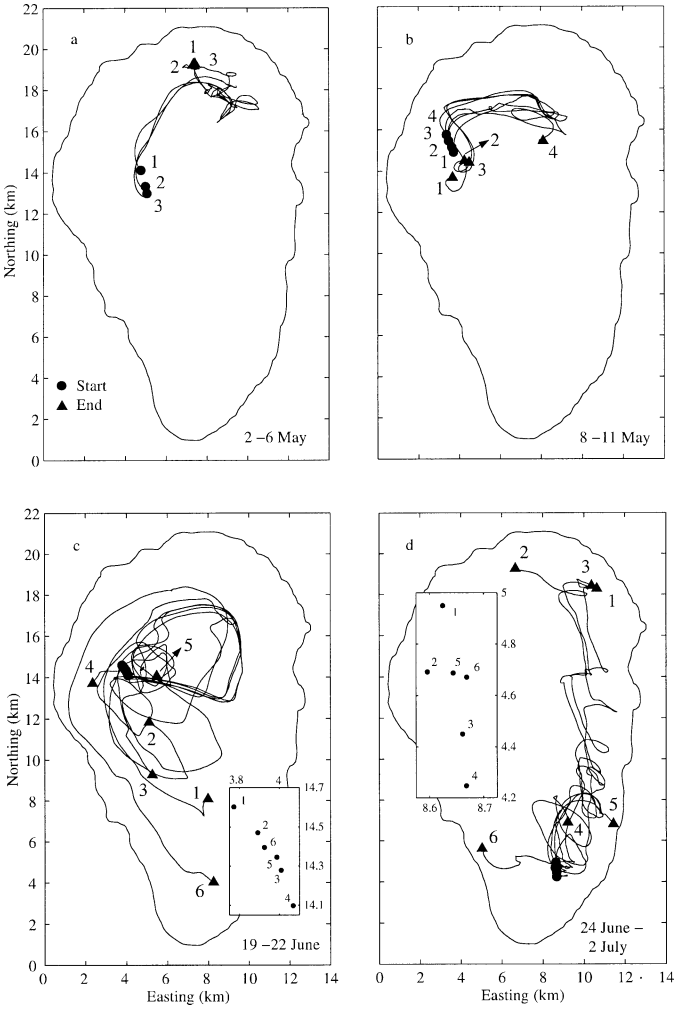

Fig. 2. Trajectories of the drifters in experiments (a) 3, (b) 4, (c) 5, and (d) 6. The dates of each experiment (2001) are given. Circles indicate locations of deployment and are magnified in the inset for experiments 5 and 6. Triangles indicate locations of retrieval. The depths of the drifters and details about their deployment are given in Table 1.

induced slippage and the finite size of the drogues were summarized, for example, by Murthy (1975) and Haynes and Barton (1991). The raw position data were checked against beaching, then low-pass filtered with a cutoff period of 15 min. Trajectories for four experiments are shown in Fig. 2. Velocities were computed by center differences, filtered, and subsampled at 15 min.

The wind speed and direction were measured at eight locations (*see* Fig. 1) for almost the entire duration of the experiments. Wind data were low-pass filtered and subsampled at 15 min, then corrected to 10-m elevation above mean water level following Amorocho and DeVries (1980). In spring the wind field was highly irregular, while the regularity of westerly sea breezes, reaching speeds in excess of 12 m s^{-1}, characterized the summer period (Fig. 3a,b). Water column temperatures were measured at six stations (*see Fig. 1*), revealing the dramatic internal wave field, with amplitudes in excess of 10 m (Fig. 4), excited by the periodic wind forcing (*see also* Antenucci et al. 2000).

Experiment 5—The analysis will focus on experiment 5 (Fig. 2c), which had the largest number of drifters deployed (six) and excellent wind and water temperature data from all stations. After being advected by a swift, wind-driven offshore current for the initial 15 h, the drifters revealed the typical cyclonic circulation first detected by Serruya (1975) and confirmed by numerical simulations of Pan et al. (2002). The horizontal convex hull (the smallest convex polygon) formed by the six drifters is shown in Fig. 5 at intervals of 15 h, along with trajectories relative to the centroid. The mean initial distance between two successive drifters was approximately 100 m (Fig. 2c, inset). By comparing the final (Fig. 5b) to the initial (Fig. 2c, inset) position of the drifters relative to their centroid, two things become apparent. First, part of the cluster's growth was due to vertical shear in the horizontal velocity field, as indicated by the trajectory of the deepest drifter (number 6, 8-m depth). The latter moved southward and away from the centroid at an average speed of 3 cm s^{-1}, reaching a final distance of 6.5 km and thus substantially increasing the apparent horizontal area of the

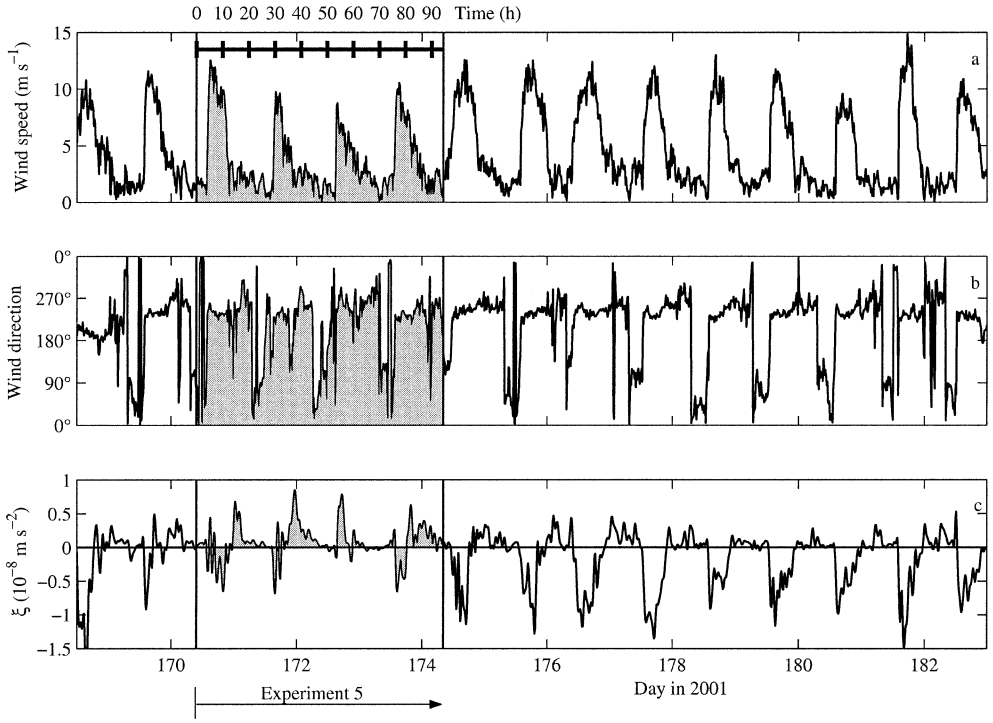

Fig. 3. (a) Wind speed and (b) direction recorded at station TF (*see Fig. 1*) and corrected to 10-m elevation above mean water level. (c) Curl of the wind stress field, from measurements at the eight stations shown in Fig. 1. The shaded area delimited by thick vertical lines indicates the period of experiment 5, for which an additional time scale in hours since deployment is given.

cluster. Interestingly, it will be shown in a later section that vertical shear dispersion was negligible despite the strength of vertical shear apparent from the behavior of drifter 6. Second, vertical shear was strongest below 5 m, as suggested by the shallowest drifter (number 5, 2.5-m depth) behaving in a similar fashion to the drifters at 5-m depth. Consideration of all six drifters increased the mean bulk horizontal dispersion coefficient by about a factor of three, but discussion will focus on the four drifters at 5 m depth, hereafter referred to as the reduced cluster.

Transport at short time scales

In this section, the effect of internal waves on the growth of the reduced cluster is investigated. Because of conservation of volume, positive (negative) vertical excursions of the thermocline associated with an internal wave correspond to convergence (divergence) events in the surface layer (the positive vertical direction being upward). For a cluster whose size is comparable to the horizontal scale of the internal wave, this translates into a contraction (expansion)

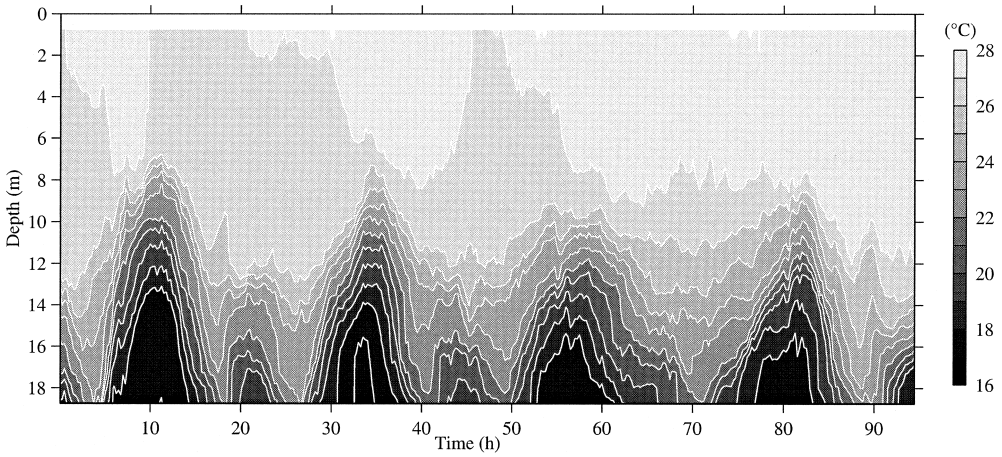

Fig. 4. Stratification at station TF (*see Fig. 1*) during experiment 5. Time is in hours from deployment of the drifters.

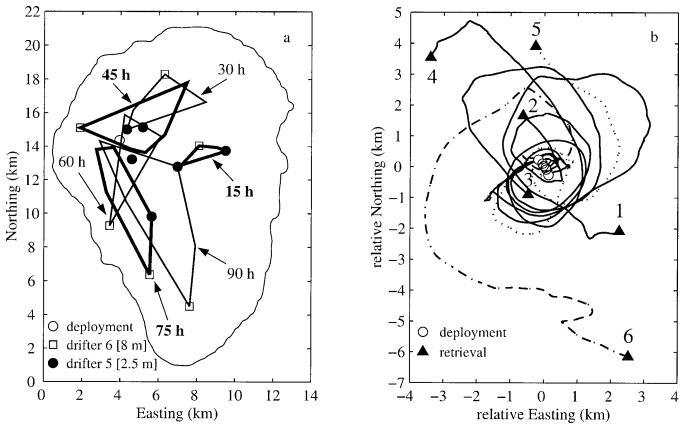

Fig. 5. (a) Convex hull (smallest convex polygon) formed by the six drifters in experiment 5, represented every 15 h from deployment. Numbers in square brackets indicate depth of deployment. The convex hull is defined as the smallest (convex) polygon including all drifters. Every second polygon has been drawn with a thick line for better visualization. (b) Trajectories of the same six drifters relative to their centroid.

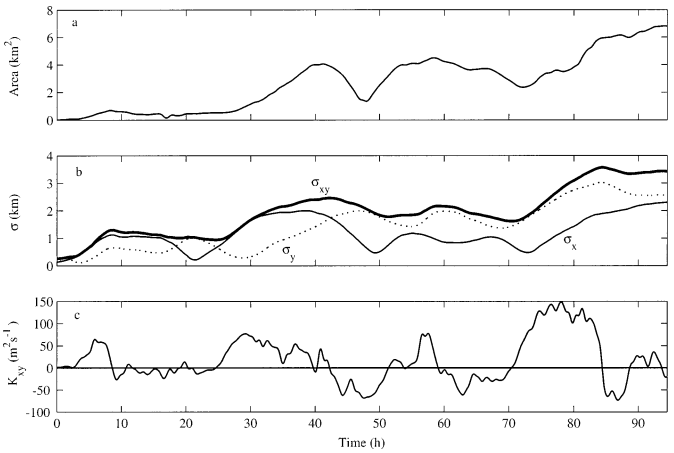

Fig. 6. (a) The area of the convex hull (smallest convex polygon) formed by the reduced cluster in experiment 5. (b) Standard deviations σ_x and σ_y along the x and y directions and two-dimensional standard deviation $\sigma_{xy} = (\sigma_x^2 + \sigma_y^2)^{1/2}$. (c) Overall dispersion coefficient $K_{xy} = 0.5\, d\sigma_{xy}^2/dt$. Time is given in hours from deployment.

proportional to the amplitude of the wave. These events strongly affect the surface layer thickness and hence the vertical wind-driven mixing and will be shown in the following to have occurred during experiment 5 from time series of the cluster's area (Fig. 6a), computed as the surface area of the convex hull, and from time series of the standard deviations of the drifters' distribution (Fig. 6b). Standard deviations, σ_x and σ_y along the x and y directions (where x and y are positive to the east and to the north, respectively) are shown together with the two-dimensional standard deviation $\sigma_{xy} = (\sigma_x^2 + \sigma_y^2)^{1/2}$. Dispersion coefficients, defined for example as $K_x = 0.5\, d\sigma_x^2/dt$ for the x direction, were also computed, and K_{xy} is shown in Fig. 6c. Their mean values were $K_x = 7.8$, $K_y = 9.3$, and $K_{xy} = 17.1$ m^2 s^{-1}.

Dispersion coefficients will be analyzed in more detail in the next section. Of interest here are the very pronounced, periodic oscillations apparent in Fig. 6a,b. After a first day characterized by very slow growth, two large divergence–convergence events were observed, beginning 28 and 48 h after deployment, respectively. During the first event the area temporarily increased by a factor of 7 in only 15 h and subsequently reduced again by 2.5 times over 7 h. A third and even larger event appeared to follow at 72 h but was unfortunately interrupted by retrieval of the drifters. These events are characterized by instantaneous horizontal growth rates that were an order of magnitude larger than the mean dispersion coefficient $K_{xy} = 17.1$ m^2 s^{-1}. The periodic nature of K_{xy} (Figs. 6c) suggests that the oscillations were caused by internal waves, with the convergence events represented by the large, negative lobes exhibited by the overall dispersion coefficient. Indeed, the period of 24 h is in good agreement with the period of the dominant internal waves (*see* Fig. 4 and Antenucci and Imberger 2001). Although these oscillations represent reversible expansions and contractions of the horizontal plane area of the clusters, they may be expected to have a large impact on the dynamics of the surface layer. For example, they modulate the thickness of the surface layer and therefore its susceptibility to vertical wind-driven mixing over times comparable to the internal waves' period. Furthermore, by periodically lifting the thermocline, they may affect the light availability for phytoplankton, whose dynamics are therefore directly influenced by the period and by the phase of the internal waves with respect to their own daily life cycle. The period of the internal waves is, in turn, a function of the Burger number (Gill 1982) and typically in the order of a day for medium-sized lakes (Antenucci and Imberger 2001). Conservation of potential vorticity will be used in a later subsection to fully describe the implications of this mechanism. First, however, the differential kinematic properties of the flow field need to be computed.

Cluster analysis—Cluster analysis proves very convenient in analyzing the large-scale properties of the flow and therefore in exploring further the effect of internal waves. Given a record of drifter velocities, cluster analysis allows computation of time series of Lagrangian velocity gradients ($\partial u/\partial x$, $\partial u/\partial y$, $\partial v/\partial x$, $\partial v/\partial y$, where u and v are the velocities in the x and y directions, respectively), considered uniform over the area of the cluster. These gradients can be combined into differential kinematic properties, defined as

$$\zeta = \partial v/\partial x - \partial u/\partial y \quad \text{vorticity} \tag{3a}$$

$$\delta = \partial u/\partial x + \partial v/\partial y \quad \text{divergence} \tag{3b}$$

$$a = \partial u/\partial x - \partial v/\partial y \quad \text{stretching deformation} \tag{3c}$$

$$b = \partial v/\partial x + \partial u/\partial y \quad \text{shearing deformation} \tag{3d}$$

Differential kinematic properties for the reduced cluster are shown in Fig. 7 and summarized in Table 2. The very large initial values of the differential kinematic properties are due to the inadequate separation of the drifters, deployed along a line (Fig. 2c, inset) with the initial purpose of capturing the influence of small variations in the cross-shore location. The initial cluster was therefore too stretched to behave two

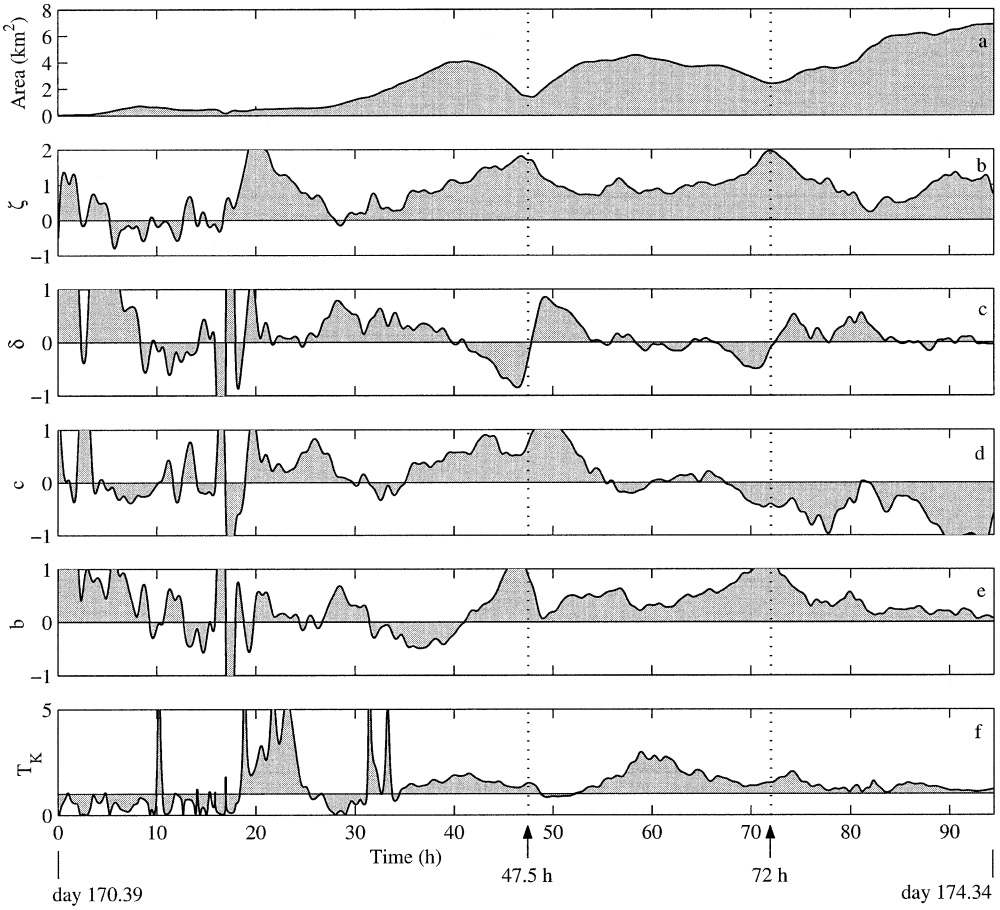

Fig. 7. (a) Area, (b)–(e) differential kinematic properties, and (f) Truesdell's kinematical vorticity number $T_K = [\zeta^2/(a^2 + b^2)]^{1/2}$, for the reduced cluster in experiment 5. The area is repeated from Fig. 6 for ease of interpretation. Among the differential kinematic properties (b) ζ is vorticity, (c) δ is divergence, (d) a is stretching, and (e) b is shearing. Units for panels (b) to (e) are 10^{-4} s^{-1}, while T_K is dimensionless. Note the different vertical scale used for vorticity. Time is in hours from deployment. The events at 47.5 and 72 h are indicated. Deployment and retrieval times are also given in days in 2001.

dimensionally, and the first 7 h are not considered in the analysis. The cluster stretched in the east–west direction for the first 2 d and in the north–south direction for the last 2 d. Horizontal divergence was positive on average, but two temporally localized periods of strong horizontal convergence were observed after 41 and 66 h of deployment, reflecting the contractions due to internal waves discussed above.

Table 2. Differential kinematic properties and kinematical vorticity number T_K during experiment 5 as computed from cluster analysis for the four drifters drogued at 5-m depth and for all six drifters. The first 7 h of the experiment have been neglected. Mean values and standard deviations are given.

		4 drifters (10^{-5} s^{-1})	6 drifters (10^{-5} s^{-1})
Stretching	a	0.4±6.0	0.8±3.8
Shearing	b	3.4±5.8	2.5±3.9
Vorticity	ζ	8.2±5.8	6.8±4.3
Divergence	δ	1.8±6.9	2.1±5.0
T_K (no units)		1.4±1.1	1.7±1.0

Vorticity was the dominant horizontal kinematic property, as seen from Fig. 7c, and assumed positive values for most of the time. Two indicators of the relative importance of the vorticity field with respect to the strain field (stretching plus shearing deformation) are the kinematical vorticity number $T_K = [\zeta^2/(a^2 + b^2)]^{1/2}$ (Truesdell 1954), where a, b, and ζ are defined in Eq. 3, and the Okubo–Weiss parameter $Q = a^2 + b^2 - \zeta^2 = (a^2 + b^2)(1 - T_K^2)$. The latter is often used to describe dispersion in two-dimensional turbulence (*see* Provenzale 1999, and references therein). When $T_K > 1$ ($Q < 0$), the vorticity field is stronger than the strain field and eddy-like structures are present (elliptic regions), while for $T_K < 1$ ($Q > 0$) the strain field dominates, corresponding to zones of convergence or divergence (hyperbolic regions) where dispersion is stronger (Klein and Hua 1990; Provenzale 1999). During experiment 5, T_K was consistently larger than one after about 18 h, with an average value of 1.5 (Table 2). For very large values of T_K,

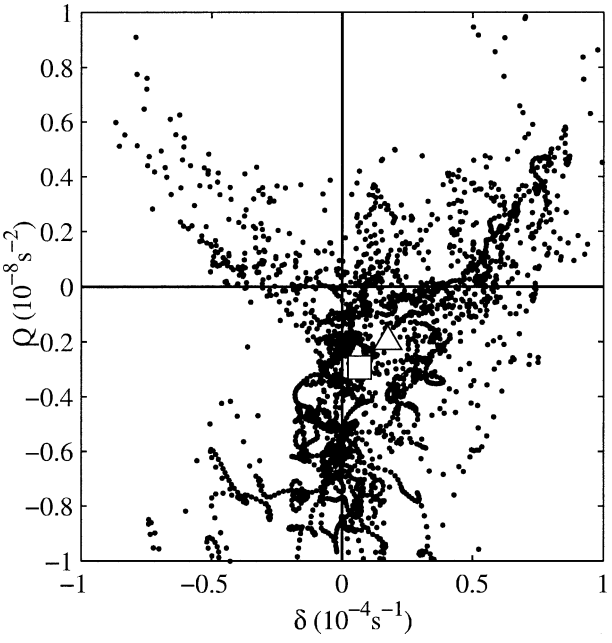

Fig. 8. The Okubo–Weiss parameter $Q = a^2 + b^2 - \zeta^2$ versus the divergence δ of the reduced cluster in experiment 5. The quantities a, b, ζ have been defined in Fig. 7. Mean values (triangle) and median values (square) are shown.

the cluster rotates almost without changing its shape, as happened from 55 to 65 h after deployment. The Okubo–Weiss parameter is plotted against divergence in Fig. 8. The median values indicate that most of the time the cluster was rotating but not diverging. Divergence was largest when the strain field dominated over the vorticity field ($T_K < 1$, $Q > 0$). Indeed, for $Q > 0$, $\langle\delta\rangle = 0.48 \times 10^{-4}$ s^{-1}, while for $Q < 0$, $\langle\delta\rangle = 0.06 \times 10^{-4}$ s^{-1}, the angular brackets denoting a time average. In the following subsection these observations are reinterpreted in terms of potential vorticity, allowing us to link the differential kinematic properties with the convergence–divergence events caused by internal waves.

Conservation of potential vorticity—A striking feature about the reduced cluster is the coincidence of two peaks in vorticity after 47 and 72 h (Fig. 7a) with two local minima in the cluster's area (Fig. 6a). This can be explained in terms of conservation of potential vorticity, whereby the vorticity is larger when the area is smaller. Following Gill (1982), potential vorticity for the surface layer, considered to be shallow and homogeneous, is defined as

$$P = \frac{f + \zeta}{h_1 - \eta} \tag{4}$$

where η is the interface displacement, positive upward, and h_1 the surface layer thickness at rest. In the absence of dissipation and following the motion, it can be shown that the potential vorticity of each fluid column evolves according to

$$\frac{DP}{Dt} = \frac{\xi + \gamma}{(h_1 - \eta)^2} \tag{5}$$

with

$$\xi = \frac{1}{\rho_w}\left(\frac{\partial \tau_y}{\partial x} - \frac{\partial \tau_x}{\partial y}\right) \tag{6a}$$

$$\gamma = \frac{1}{\rho_w}\left(\tau_y \frac{\partial \eta}{\partial x} - \tau_x \frac{\partial \eta}{\partial y}\right)(h_1 - \eta)^{-1} \tag{6b}$$

where $(\tau_x, \tau_y) = \rho_a C_d (u_w^2 + v_w^2)^{1/2}(u_w, v_w)$ is the wind stress, (u_w, v_w) is the wind velocity at 10 m height, $C_d = 1.2 \times 10^{-3}$ is a drag coefficient, and ρ_w and ρ_a are representative water and air densities, respectively. Equation 5 states that potential vorticity of fluid columns in the surface layer can be modified by wind forcing but is otherwise conserved.

To estimate P from Eq. 4, the vorticity ζ determined from cluster analysis (Fig. 7c) was used. The interface displacement η was determined from thermistor chain data and represented the quantity with the largest uncertainties, involving a spatial interpolation of the temperature profile at the location of the drifters' centroid. Since potential vorticity is conserved in a Langrangian sense, all quantities in Eq. 5 have to be computed following the fluid column located at the centroid. With the 26.2°C isotherm representative of the thermocline (*see Fig. 4*), the position of this isotherm in time at the instantaneous location of the centroid defines the instantaneous thickness of the fluid column ($h_1 - \eta$ in Eq. 4) in the absence of heat inputs (i.e., when isotherms are material surfaces). However, when surface heating or cooling are present, their contribution to isotherm displacement has to be separated out in order to determine the thickness of the fluid column. This was done as follows. At any given time step, the temperature profile at the position of the centroid was interpolated from all thermistor chains (except *T*7, too distant from the cluster), with weighting factors proportional to the inverse squared distance between the centroid and each chain. The variation in the surface temperature at the position of the centroid from the previous time step was used to compute the heat input (solar radiation data might have been used instead, involving one further spatial interpolation, but given the resulting small influence of surface heat inputs this was not necessary). This heat input allowed the computation of the temperature variation at the base of the fluid column (with a light extinction coefficient of 0.5 m^{-1}; the total temperature variation over experiment 5 resulted in less than 0.02°C. The new temperature was then used to find the new thickness of the fluid column.

The thickness of the centroid fluid column is represented in Fig. 9a as a function of time, and its mean value (11.0 m) was taken as h_1. This yielded a potential vorticity for the lake at rest of $P_0 = f/h_1 = 0.090f$ m^{-1}. The interface displacement η is the difference between h_1 and the instantaneous interface depth. The evolution of P is shown in Fig. 9b. After an initial increase, potential vorticity settles to an approximately constant value of around 0.2. Let us assume, as a first approximation, that P was constant after 14 h from deployment, thereby neglecting the wind forcing in Eq. 5. The value of P that best fits Eq. 4 is $P = 0.196f$ m^{-1}, more

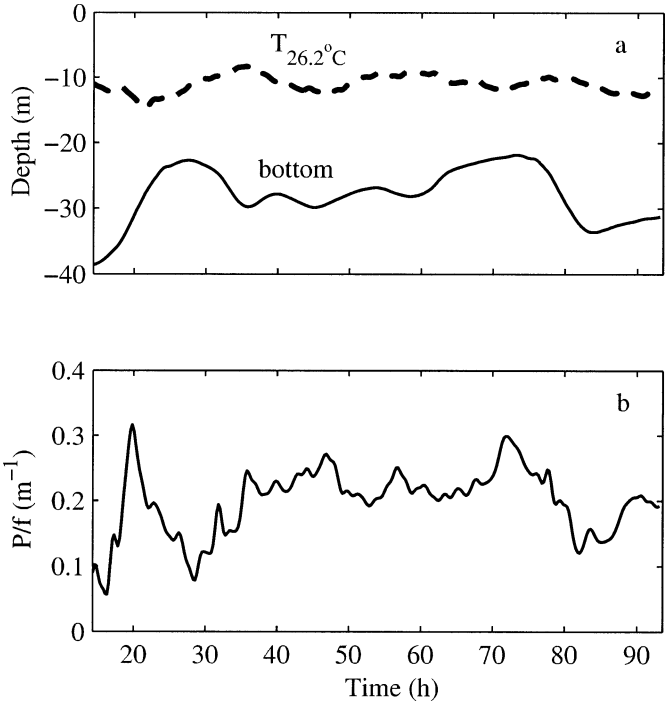

Fig. 9. (a) Depth of the interface η (dashed line) and of the bottom (solid line) as seen by the centroid of the reduced cluster in experiment 5. The interface is defined as the depth of a water parcel initially lying on the 26.2°C isotherm and is computed by interpolation from the six thermistor chains (*see Fig. 1*). The depth of the bottom is interpolated from the bathymetry of the lake. (b) Potential vorticity P of the reduced cluster normalized by the planetary vorticity f. Note that the potential vorticity at rest is $P_0 = 0.090f$ m^{-1}. Time is given in hours from deployment.

than twice the potential vorticity at rest. Using Eq. 4 with $P = P$, the relation $DP/Dt = 0$ can be rewritten as

$$\frac{\zeta}{f} = \frac{\bar{P}(h_1 - \eta)}{f} - 1 \tag{7}$$

The left- and right-hand sides of this equation are compared in Fig. 10. Considering the uncertainties in the determination of η, the agreement is remarkable, implying that potential vorticity was conserved over time scales of a few days.

As a verification, a different approach was adopted. Gill (1982) showed that when potential vorticity is conserved the divergence can be computed from the vorticity equation as

$$\delta = -\frac{1}{\zeta + f}\frac{d\zeta}{dt} \tag{8}$$

The two estimates of divergence obtained by substituting the differential kinematic properties of the reduced cluster (Fig. 7) in this equation are compared in Fig. 11 for the period ranging from 41 to 82 h. The right-hand side has been filtered at 3 h to smooth out the noise introduced by the numerical time derivative. From 62 to 82 h the quantitative agreement is again surprisingly good. This reflects the fact that the divergence field of the internal waves forced the cluster to expand and contract, ultimately increasing or decreasing its relative vorticity, so that potential vorticity was

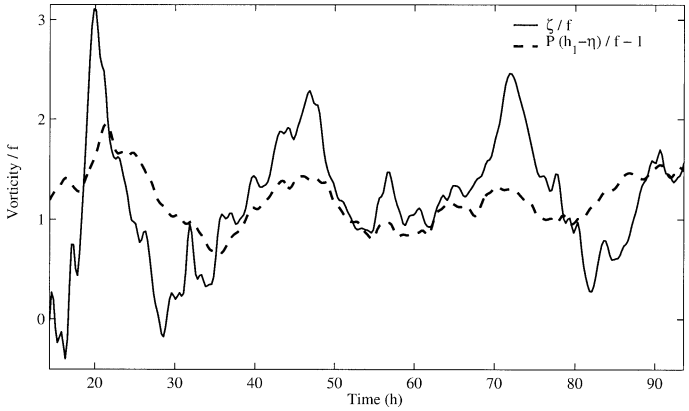

Fig. 10. Vorticity of the reduced cluster in experiment 5 computed from cluster analysis (solid line), compared to that computed from conservation of potential vorticity P in Eq. 7 (dashed line). The interface displacements η are taken from Fig. 9. Vorticity has been normalized by the planetary vorticity f. Time is given in hours from deployment.

conserved. This mechanism is effective when the size of the cluster is comparable to the wavelength of the internal waves, which scales like the Rossby radius of deformation $R = c/f$ (Gill 1982). At the latitude of Lake Kinneret $f = 7.9 \times 10^{-5}$ s^{-1}, while from thermistor chain data $c \approx 0.33$ m s^{-1} (*see also* Antenucci et al. 2000), yielding $R \approx 4.2$ km. For the two events at 47.5 and 72 h discussed above, Fig. 6b shows that the size of the cluster was comparable to the Rossby radius. As a confirmation, we note that a further peak in vorticity, 20 h after deployment, was not matched by a local minimum in the cluster's area (Fig. 6a): since the size of the cluster at this point was still much smaller than the scale of the internal waves, the cluster did not respond to the divergence field of the waves but was simply advected by them. This discussion also sheds light on the effects of changing the initial area of the cluster, with a larger (smaller) initial area implying the cluster would begin responding to the internal wave field earlier (later).

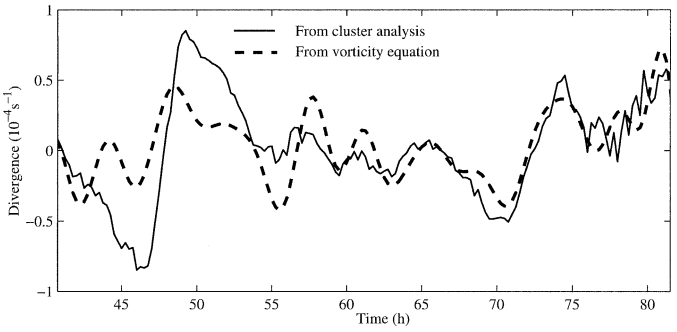

Fig. 11. Divergence of the reduced cluster in experiment 5 computed from cluster analysis (solid line), compared to that computed from the vorticity equation, Eq. 8 (dashed line). The second signal has been low-pass filtered at 3 h to smooth out the noise introduced by the numerical time derivative. Time is given in hours from deployment.

The wind forcing—An estimate of the effect of the wind field on the potential vorticity balance (Eq. 5) was attempted using the wind data from eight stations (*see Fig. 1*) to evaluate the two forcing terms in Eq. 6. Cluster analysis applied to the wind stress field in an Eulerian sense (the positions of the eight stations being fixed) allowed the computation of the wind stress curl, shown in Fig. 3c. During experiment 5, both the magnitude of the wind speed (Fig. 3a) and the wind stress curl (Fig. 3c) were atypically weak for summer conditions. Therefore, the 2 week period represented in Fig. 3 was considered more representative for the effects of wind forcing. The afternoon sea breeze was typically characterized by a strong, negative wind stress curl, contradicting findings by Pan et al. (2002).

Estimating $\xi = -5 \times 10^{-9}$ m s^{-2} from Fig. 3c and $(h_1 - \eta)^2 \approx h_1^2$ yields a rate of change of potential vorticity of $5f \times 10^{-7}$ m^{-1} s^{-1}, which, for a typical value of $P = 0.1f$ m^{-1} (Fig. 9b), indicates that the wind field would have influenced potential vorticity on time scales in the order of 2 d. While recent numerical simulations by Marti and Imberger (pers. comm.) seem to substantially confirm this estimate, suggesting a spin-up time in the order of 1 d, several uncertainties remain. First, the wind stress curl was not steady over any 2 d (Fig. 3c). Second, the influence of the shallow regions (depth less than h_1) is not taken into account by this scaling analysis. Third, the second forcing term in Eq. 5, representing the coupling of a uniform wind with interface gradients, was potentially of the same order as the first one for wind speeds as small as 5 m s^{-1} as seen by assuming an interface gradient of 10^{-3} (a 10 m interface displacement over 10 km) and $(h_1 - \eta)^3 \approx h_1^3$. These uncertainties make it difficult to compute a more precise time scale over which wind forcing affected the potential vorticity balance in the surface layer.

Dispersion at intermediate time scales

Overall observed dispersion—While experiment 5 only spanned a few internal wave periods, it is evident from Fig. 6a,b that underlying the periodic convergence–divergence events there was a net growth in the size of the cluster. Indeed, we found an average value of $K_{xy} = 17.1$ m^2 s^{-1} from Fig. 6c, small compared with the instantaneous growth rates, but significant in view of the fact that internal waves do not cause any mean net growth. In this section we investigate the mechanism responsible for this overall dispersion.

While the standard deviations of the cluster (*see Fig. 6b*) clearly did not obey a simple linear growth rate, it is nevertheless interesting to see whether Okubo's empirical formulation (Eq. 2) describes the growth rate of the cluster appropriately as a function of its size. This was done in Fig. 12 by comparing the two estimates for K_a from Eqs. 1 and 2, where the relation for Gaussian distributions $\sigma_r^2 = 2\sigma_{\max}\sigma_{\min}$ (Murthy 1976) has been used. The reasonably good agreement that can be observed implies the size of the cluster grew like $d_r = 0.7 \times 10^{-2}\, t^{1.11}$, which is confirmed by the approximately linear increase in time at a rate of 1 cm s^{-1} exhibited by the mean distance of the drifters from their centroid (not shown).

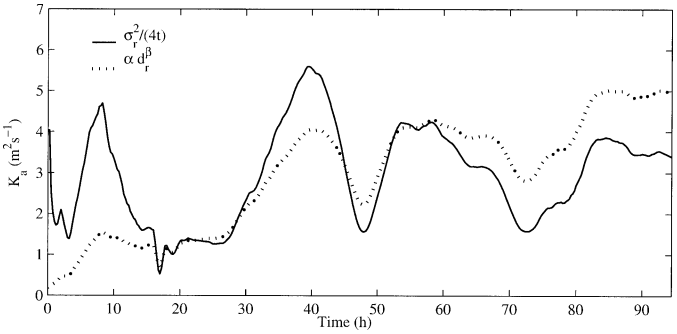

Fig. 12. The apparent radially symmetric dispersion coefficient for the reduced cluster in experiment 5 as estimated from Eq. 1 using $\sigma_r^2 = 2\sigma_{\max}\sigma_{\min}$ (Murthy 1976) (solid line) and from Eq. 2 with $\alpha = 3.20 \times 10^{-4}$ m$^{0.9}$ s^{-1} and $\beta = 1.10$ (Lawrence et al. 1995) (dashed line). Time is given in hours from deployment.

A common theoretical interpretation for the success of Eq. 2 is based on Richardson's 4/3 law (Richardson 1926; Batchelor 1952). As a cloud grows, larger and larger eddies contribute to its dispersion, causing the dispersion coefficient to grow with the size of the cloud. Okubo (1971) showed that for a wide range of experiments $\beta = 4/3$ within each experiment, and recently Stacey et al. (2000) suggested this value to hold also for the near-coastal environment. When data from several experiments are combined, β is somewhat less than 4/3, specifically 1.10 (Lawrence et al. 1995). However, it seems unlikely that the range of eddies postulated by Richardson's law would develop in the surface layer of a stratified, bounded basin of compact shape like Lake Kinneret, where the largest eddies are likely to scale with the depth of the surface layer (*see*, e.g., Csanady 1963). Therefore, while there is no conclusive evidence of this latter point, it is suggested that an alternative mechanism, namely unbounded horizontal shear dispersion, was responsible for the observed dispersion rates, while also yielding a 4/3 power law dependence similar to Eq. 2 (Fischer et al. 1979). This hypothesis is supported by the large values of the horizontal velocity gradients, exceeding by almost one order of magnitude those measured in the ocean (e.g., Molinari and Kirwan 1975; Sanderson 1995; Richez 1998). Before attempting to estimate the magnitude of horizontal shear dispersion, however, a quantification of the diffusivities due to small-scale motions is required.

Observed diffusivities—An estimate of the diffusivities associated with the small-scale motions, interpreted as the residual velocities computed from cluster analysis, was obtained in two ways. Following Okubo and Ebbesmeyer (1976), we can take the turbulence intensity to be proportional to the standard deviation of the residual velocities (σ_u, σ_v) and the mixing length scale proportional to the standard deviation of the drifters' displacements (σ_x, σ_y), yielding $\kappa_x = c\sigma_x\sigma_u$, $\kappa_y = c\sigma_y\sigma_v$, where c is a constant between 0.1 and 1 (Okubo and Ebbesmeyer 1976). With $c = 0.1$ we obtain the mean values $\kappa_x = 1.9$ and $\kappa_y = 3.0$ m^2 s^{-1}.

Since these values are dependent on the choice of c, an alternative estimate was obtained from the Lagrangian statistics of the residual motions. A stationarity test using the

method of reverse arrangements (Bendat and Piersol 2000) with 100 sampling intervals showed that residual velocities were stationary at the 5% level of significance. Therefore, assuming the statistical properties were also homogeneous, the theory by Taylor (1921) (*see also* Pal et al. 1998) can be applied, providing an estimate for the Lagrangian time (T_x = 2.4 h, T_y = 4.1 h) and length scales (L_x = 100 m, L_y = 160 m). To account for the finite length of the trajectories, the autocorrelation function was integrated only up to the time of first zero crossing, effectively computing upper bounds to the true Lagrangian scales (Colin de Verdiere 1983). To achieve statistical significance despite the small number of trajectories, the segmentation method was used, taking advantage of stationarity and homogeneity (Poulain and Niiler 1989; Pal et al. 1998). Since the motion of a drifter becomes uncorrelated after a time in the order of the Lagrangian time scale, trajectories were restarted every 10 h, increasing the number of realizations from 4 to 28. Diffusivities were then computed for each direction as $\kappa = L^2/T$, yielding κ_x = 1.2 and κ_y = 1.8 m^2 s^{-1}. These values are 40% smaller than those computed above, but substantially confirm that the order of magnitude of our estimate is correct.

Unbounded horizontal shear dispersion—Unbounded horizontal shear dispersion affects clouds whose extent has not yet reached the horizontal bounds of the domain. The dispersion coefficient for a unidirectional shear flow along the x direction is (Fischer et al. 1979)

$$K_x = 1.5c_2(\partial u/\partial y)^2\kappa_y t^2 \tag{9}$$

An equivalent expression applies for the y direction, and the formulation holds equally for a cluster of drifters, which by definition diffuse laterally. Using c_2 = 0.037 as for point sources (Saffman 1962), κ_x = 1.2 and κ_y = 1.8 m^2 s^{-1} as found earlier from Lagrangian statistics, and the mean shear values $(\partial u/\partial y, \partial v/\partial x) = (-2.4, 5.8) \times 10^{-5}$ s^{-1} from cluster analysis, we found K_x = 6.7, K_y = 25.9, and K_{xy} = 32.6 m^2 s^{-1} for the duration of experiment 5. These values are somewhat larger, but of the same order, as the overall observed dispersion coefficients given above (*see Fig. 6c*).

As a confirmation of this, and to further exploit the detailed knowledge of the time series of the horizontal shear, we applied the approach proposed by Smith (1982). With a linear shear $\partial u/\partial y$ of arbitrary time dependence, the exact solution of the two-dimensional advection–diffusion equation yields (*see also* Sundermeyer and Ledwell 2001)

$$\sigma_x^2 = 2\kappa_y \int_0^t G^2\, dt' \tag{10a}$$

$$G = \frac{1}{t - \tilde{t}} \int_0^t (t' - t)\frac{\partial u}{\partial y}(t')\, dt' \tag{10b}$$

where $\tilde{t} = -\sigma_{x_0}^2/2\kappa_y$ and $\sigma_{x_0}^2$ is the initial variance of the cluster along x. An equivalent expression holds for the y direction. Using the linear shear time series from cluster analysis (subsampled at 6 min for computational efficiency), we found mean values of K_x = 15.8, K_y = 45.7, K_{xy} = 61.5 m^2 s^{-1} from Eqs. 10 for the duration of experiment 5. While these values are larger than those estimated from Eq. 9, it has to be considered that a linear shear yields an upper bound to shear dispersion (Sundermeyer and Ledwell 2001). We conclude that horizontal shear dispersion rates are of the same order of the observed dispersion rates, suggesting horizontal shear dispersion to be an important mechanism for the growth of a cloud in the surface layer.

Discussion

The arguments presented shed new light on the processes governing the growth of a cloud in the surface layer of stratified lakes. Over short time scales, in the order of a day in medium-sized lakes, internal waves provide the primary mechanism by which divergence and convergence events modify the horizontal area of a cloud. These events are characterized by instantaneous growth rates that are an order of magnitude larger than the mean dispersion coefficient, making the growth of a cloud in the surface layer a very dynamic process on short time scales, as already observed by Stevens et al. (1995). Although they are reversible, implying they cancel out in the mean, these events modify the thickness of the surface layer, making it more (convergent events) or less (divergent events) susceptible to wind mixing. These events are also likely to influence phytoplankton dynamics significantly, since by lifting (depressing) the thermocline periodically they expose phytoplankton to higher (lower) light availability. The internal wave field modulates the vorticity field, so as to satisfy conservation of potential vorticity. Divergence events correspond to a loss of positive relative vorticity, as observed also by Reed (1971) over a 6-h period in the Alaskan stream. The rotation of the cluster then acts as an antidivergent mechanism, and most of the growth of the cloud occurs during periods of low vorticity (Fig. 8). Incidentally, a similar result applies for two-dimensional turbulence (Provenzale 1999). Over time scales larger than 2 d, an order of magnitude analysis suggests that the potential vorticity balance is affected by the wind stress curl. However, the uncertain estimate of the wind-forcing terms makes it impossible to draw more precise conclusions.

Over intermediate time scales, of the order of a few internal wave periods, irreversible dispersion is well predicted by an empirical formulation like Eq. 2, relating the dispersion coefficient of a cloud to its size. While Richardson's 4/3 law is often invoked to justify the success of Eq. 2, its use does not seem justified in a stratified, compact lake, where there is no evidence of the wide range of eddies required for its validity. Instead, it is suggested that the dominating mechanism in the surface layer is horizontal shear dispersion, which is also associated with a 4/3 power law formulation (Fischer et al. 1979). Horizontal shear dispersion is important in the lake because of the large horizontal velocity gradients, which exceed by almost one order of magnitude those measured in the ocean (e.g., Molinari and Kirwan 1975; Sanderson 1995; Richez 1998). Since it is a large-scale mechanism, dependent on the mean circulation, it is readily apparent how a better understanding of the circulation in stratified lakes is necessary to improve predictions of dispersion rates. The present study showed that La-

grangian drifter experiments and cluster analysis are well suited to accomplish this.

A second, completely deterministic dispersion mechanism that is possibly important but difficult to assess quantitatively from the present data is pseudochaotic advection. Stocker and Imberger (2003) showed that the superposition of internal waves and a steady circulation can lead to enhanced dispersion in certain regions of the lake whose location is determined by the topology of the steady flow field and in particular by its hyperbolic points. The presence of a steady geostrophic circulation consisting of two oppositely rotating gyres is suggested by the linear inviscid solution to the uniformly forced problem (Stocker and Imberger 2003) and by numerical investigations (Serruya et al. 1984; Herman 1989). While the variability in the wind field and the effects of bottom friction and topography (*see* Serruya et al. 1984; Herman 1989) do not warrant a detailed description of the temporal and spatial variation of the enhanced dispersion regions, the location of the hyperbolic points agrees with the recirculation regions observed in the north and south of the lake (Fig. 2a,d; *see also* Pan et al. 2002). For a tracer cloud of initial size d_0, a dispersion coefficient over time t can be estimated as $K_{ch} = d_0^2 \lambda e^{2\lambda t}$ (Stocker and Imberger 2003), where λ is the finite time Lyapunov exponent. For typical values of stratification and wind forcing, regions with $\lambda \approx 0.05f$ can be expected to develop in the lake (Stocker and Imberger 2003). Over a time of 2 d, a cloud having an initial size of 1 km would have $K_{ch} = 15$ m^2 s^{-1}, comparable to the observed dispersion rate. While more detailed studies would be required to verify this estimate, it is interesting to note that pseudochaotic advection, like horizontal shear dispersion, is keyed to the large-scale circulation of the lake.

Turbulent dispersion can be shown to be negligible by a simple scaling argument. For a cloud encompassing all scales of turbulent motion in a wind-driven surface layer of depth h_1, the turbulent dispersion coefficient scales like $h_1 u_*$ (Imberger and Monismith 1986), where h_1 has been taken as the horizontal scale of the largest eddies (as mentioned above) and the wind shear velocity u_* has been taken as their velocity scale. This is in the order of 0.05 m^2 s^{-1}, two orders of magnitude lower than the observed dispersion coefficient, indicating that the eddies are too small to significantly contribute to dispersion.

Vertical shear dispersion also appears to be negligible. While drifters are not affected by vertical shear dispersion, since they do not diffuse vertically, it is interesting to estimate the importance of this mechanism for a cloud whose vertical diffusivity is κ_z. Before being mixed over the depth h_1 of the surface layer in a time $T_V = 0.4 h_1^2 \kappa_z^{-1}$ (Fischer et al. 1979), the apparent horizontal growth of the cloud is affected by unbounded vertical shear dispersion. While no precise calculation is warranted by the available data, an order of magnitude analysis in which vertical shear was estimated from the differential motion of drifters at different depths (*see Table 1*) indicated that unbounded vertical shear dispersion was at least one order of magnitude smaller than the observed mean value. On the other hand, bounded vertical shear dispersion did not have the time to set in, as the following argument shows. Data collected with a portable flux profiler from 21 June to 3 July 2001 have been used to compute κ_z. Averaging 1,394 measurements from the surface layer (depths between 2 and 11 m) made on several days from 1100 h to 2200 h yielded $\kappa_z = 1.1 \times 10^{-4}$ m^2 s^{-1}, which can be considered an upper bound since sampling encompassed the periods of strongest wind. This results in a lower bound for T_V of 5.6 d, too long a time for the vertical shear to remain steady. This suggests that for typical surface layer conditions vertical shear dispersion can be dismissed as negligible, in line with the experiments by Stevens et al. (1995) in Kootenay Lake and by Sundermeyer and Ledwell (2001) over the continental shelf. Stevens et al. (1995) concluded that the missing dispersion rates were due to horizontal shear, while Sundermeyer and Ledwell (2001) pointed out the significant role of shearing and straining on horizontal scales of 1 to 10 km. Both conclusions are in agreement with our findings.

References

Amorocho, J., and J. J. DeVries. 1980. A new evaluation of the wind stress coefficient over water surfaces. J. Geophys Res. **85:** 433–442.

Antenucci, J. P., and J. Imberger. 2001. Energetics of long interval gravity waves in large lakes. Limnol. Oceanogr. **46:** 1760–1773.

———, ———, and A. Saggio. 2000. Seasonal evolution of the basin-scale internal wave field in a large stratified lake. Limnol. Oceanogr. **45:** 1621–1638.

Batchelor, G. K. 1952. Diffusion in a field of homogeneous turbulence. II. The relative motion of particles. Proc. Cambridge Phil. Soc. **48:** 345–362.

Bendat, J. S., and A. G. Piersol. 2000. Random data: analysis and measurement procedures. Wiley-Interscience.

Bowden, K. F. 1965. Horizontal mixing in the sea due to a shearing current. J. Fluid Mech. **21:** 83–95.

Colin de Verdiere, A. 1983. Lagrangian eddy statistics from surface drifters in the eastern North Atlantic. J. Mar. Res. **41:** 375–398.

Csanady, G. T. 1963. Turbulent diffusion in Lake Huron. J. Fluid Mech. **17:** 360–384.

Dever, E. P., M. C. Hendershott, and C. D. Winant. 1998. Statistical aspects of the surface drifter observations of circulation in the Santa Barbara channel. J. Geophys. Res. **103:** 24781–24797.

Fischer, H. B., E. J. List, R. C. Y. Koh, J. Imberger, and N. H. Brooks. 1979. Mixing in inland and coastal waters. Academic.

Freeland, H., P. Rhines, and T. Rossby. 1975. Statistical observations of the trajectories of neutrally buoyant floats in the North Atlantic. J. Mar. Res. **33:** 383–304.

Gill, A. E. 1982. Atmosphere-ocean dynamics. Academic.

Hayne, R., and E. D. Barton. 1991. Lagrangian observations in the Iberian coastal transition zone. J. Geophys. Res. **96:** 14731–14741.

Herman, G. 1989. The time dependent response of Lake Kinneret to an applied wind stress and hydraulic flow. Advection of suspended matter. Arch. Hydrobiol. **115:** 41–57.

Imberger, J., and S. Monismith. 1986. Appendix: A model for deepening due to upwelling when $W > 1$. J. Fluid Mech. **171:** 432–439.

Klein, P., and B. L. Hua. 1990. The mesoscale variability of the sea surface temperature: An analytical and numerical model. J. Mar. Res. 48: 729–763.

Krauss, W., and C. W. Böning. 1987. Lagrangian properties of

eddy fields in the North Atlantic as deduced from satellite-tracked buoys. J. Mar. Res. **45:** 259–291.

LAWRENCE, G. A., K. I. ASHLEY, N. YONEMITSU, AND J. R. ELLIS. 1995. Natural dispersion in a small lake. Limnol. Oceanogr. **40:** 1519-1526.

LIST, E. J., G. GARTRELL, AND C. D. WINANT. 1990. Diffusion and dispersion in coastal waters. J. Hydraul. Eng. **11:** 1158–1179.

MOLINARI, R., AND A. D. J. KIRWAN. 1975. Calculations of differential kinematic properties from Lagrangian observations in the Western Caribbean Sea. J. Phys. Oceanogr. **5:** 483–491.

MURTHY, C. R. 1975. Dispersion of floatables in lake currents. J. Phys. Oceanogr. **5:** 193–195.

———. 1976. Horizontal diffusion characteristics in Lake Ontario. J. Phys. Oceanogr. **6:** 76–84.

MUZZI, R. W., AND M. J. MCCORMICK. 1994. A new global positioning system drifter buoy. J. Gt. Lakes Res. **3:** 1–4.

OKUBO, A. 1971. Oceanic diffusion diagrams. Deep-Sea Res. **18:** 789–802.

———, AND C. C. EBBESMEYER. 1976. Determination of vorticity, divergence and deformation rates from analysis of drogue observations. Deep-Sea Res. **23:** 345–352.

OKUMURA, Y., AND S. ENDOH. 1995. Telemetry Lagrangian measurements of water movement in lake using GPS and MCA. Trans. Soc. Instrum. Control Eng. **31:** 1324–1328.

PADUAN, J. D., AND P. P. NIILER. 1993. Structure of velocity and temperature in the Northeast Pacific as measured with Lagrangian drifters in fall 1987. J. Phys. Oceanogr. **23** 585–600.

PAL, K. P., R. MURTHY, AND R. E. THOMSON. 1998. Lagrangian measurements in Lake Ontario. J. Gt. Lakes Res. **24:** 681–697.

PALMER, M. D., R. JARVIS, AND L. THOMPSON. 1987. Drogue-cluster and dye-dispersion measurements. Can. J. Civ. Eng. **14:** 320–326.

PAN, H., R. AVISSAR, AND D. B. HAIDVOGEL. 2002. Summer circulation and temperature structure of Lake Kinneret. J. Phys. Oceanogr. **32:** 295–313.

PEETERS, F. 1994. Horizontale Mischung in Seen (Horizontal mixing in lakes). Ph.D. thesis, Eidgenossische Technische Hochschule, Zurich.

———, A. WUEST, G. PIEPKE, AND D. M. IMBODEN. 1996. Horizontal mixing in lakes. J. Geophys. Res. **101:** 18361–18375.

POULAIN, P. M., AND P. P. NIILER. 1989. Statistical analysis of the surface circulation in the California current system using satellite tracked drifters. J. Phys. Oceanogr. **19:** 1588–1603.

PROVENZALE, A. 1999. Transport by coherent barotropic vortices. Annu. Rev. Fluid Mech. **31:** 55–93.

QUAY, P. D., W. S. BROECKER, R. H. HESSLEIN, E. J. FEE, AND D. W. SCHINDLER. 1979. Whole lake tritium spikes to measure horizontal and vertical mixing rates, p. 175–193. *In* Isotopes in lake studies. International Atomic Energy Agency.

REED, R. K. 1971. An observation of divergence in the Alaskan stream. J. Phys. Oceanogr. **1:** 282–283.

RICHARDSON, L. F. 1926. Atmospheric diffusion shown on a distance-neighbour graph. Proc. R. Soc. Lond. A **110:** 709–737.

RICHEZ, C. 1998. The West Spitsbergen Current as seen by SOFAR floats during the ARCTEMIZ 88 Experiment: Statistics, differential kinematic properties, and potential vorticity balance. J. Geophys. Res. 103: 15539–15565.

SAFFMAN, P. G. 1962. The effect of wind shear on horizontal spread from an instantaneous ground source. Q. J. R. Meteorol. Soc. **88:** 382–393.

SANDERSON, B. G. 1987. An analysis of Lagrangian kinematics in Lake Erie. J. Gt. Lake Res. **13:** 559–567.

———. 1995. Structure of an eddy measured with drifters. J. Geophys. Res. **100:** 6761–6776.

———, AND A. OKUBO. 1986. An analytical calculation of two-dimensional dispersion. J. Oceanogr. Soc. Jpn. **42:** 139–153.

SERRUYA, S. 1975. Wind, water temperature and motions in Lake Kinneret: General pattern. Verh. Int. Verein. Limnol. **19:** 73–87.

———, E. HOLLAN, AND B. BITSCH. 1984. Steady winter circulations in Lake Constance and Kinneret driven by wind and main tributaries. Arch. Hydrobiol. **1:** 33–110.

SMITH, R. 1982. Dispersion of tracers in the deep ocean. J. Fluid Mech. **123:** 131–142.

STACEY, M. T., E. A. COWEN, T. M. POWELL, E. DOBBINS, S. G. MONISMITH, AND J. R. KOSEFF. 2000. Plume dispersion in a stratified, near-coastal flow: Measurements and modeling. Cont. Shelf Res. **20:** 637–663.

STEVENS, C., P. F. HAMBLIN, G. A. LAWRENCE, AND F. M. BOYCE. 1995. River-induced transport in Kootenay Lake. ASCE J. Env. Eng. **121:** 830–837.

STOCKER, R., AND J. IMBERGER. 2003. Energy partitioning and horizontal dispersion in a stratified rotating lake. J. Phys. Oceanogr. **33:** 512–529.

SUNDERMEYER, M. A., AND J. R. LEDWELL. 2001. Lateral dispersion over the continental shelf: Analysis of dye release experiments. J. Geophys. Res. **106:** 9603–9621.

TAYLOR, G. I. 1921. Diffusion by continuous movements. Proc. Lond. Math. Soc. **A20:** 196–211.

TRUESDELL, C. 1954. The kinematics of vorticity. Indiana Univ. Press.

Received: 5 March 2002
Accepted: 30 December 2002
Amended: 23 January 2003